Int. J. Solids Structures Vol. 28, No. 2, pp. 249–263, 1991
Printed in Great Britain.

0020-7683/91 $3.00 + .00
© 1991 Pergamon Press plc

A GENERAL SOLUTION TO THE ANTIPLANE PROBLEM OF AN ARBITRARILY LOCATED ELLIPTICAL HOLE NEAR THE TIP OF A MAIN CRACK

S. X. GONG and S. A. MEGUID
Department of Mechanical Engineering, University of Toronto, 5 King's College Road, Toronto, Ontario, Canada M5S 1A4

(*Received* 2 *April* 1990; *in revised form* 7 *November* 1990)

Abstract—A general solution is obtained to the problem of the interaction between a main crack and an arbitrarily located and oriented elliptical hole near its tip under mode III loading conditions. The analysis is based on the complex potentials for the antiplane problem and the superposition principle. The stress intensity factor at the main crack is obtained in a general series form and approximate closed-form solutions are also derived using a perturbation procedure. The present solution is shown to coincide with Taylor expansion of exact solutions for collinear elliptical holes with specific aspect ratios. Numerical examples are provided to show the effect of the geometry, location and orientation of the microdefect on the stress intensity factor of the main crack. The present work should provide a valuable insight into main crack microdefect interaction phenomena in brittle materials.

1. INTRODUCTION

Unlike ductile materials where crack propagation is accompanied by crack-tip plasticity, the onset of a main crack extension in brittle materials is mainly governed by microcrack formation in a zone ahead of the crack-tip; see, e.g., Hoagland *et al.* (1973), Claussen *et al.* (1977), Evans and Faber (1984) and Rühle *et al.* (1987). This near-tip microcracking has been regarded as being one of the principle mechanisms which influences main crack growth in brittle materials.

Two approaches are generally adopted in the development of analytical models to predict the behaviour of a main crack in the presence of a microcracking zone. These are: (i) the continuum damage mechanics model and (ii) the discrete main crack–microcrack interaction model. In the continuum damage model, the microcracking region is described by a different constitutive equation, with a reduced effective modulus, from that corresponding to the parent material. This reduction in modulus has two counteracting effects. On one hand, it contributes to the reduction in the near-tip stresses thus leading to a shielding effect. On the other hand, it enables the main crack to grow more readily, thus leading to a reduction in resistance to fracture. The resulting enhancement or degradation of the toughness of the material would ultimately depend upon the net outcome of the above two effects. Examples of the continuum mechanics models include the work of Evans and Fu (1985), Ortiz (1987, 1988), Charalambides and McMeeking (1987) and Hutchinson (1987).

The discrete main crack–microcrack interaction model relies on the development of approximate solutions to multiple microcracks in the vicinity of a main crack; see, e.g., the work of Hoagland and Embury (1980), Chudnovsky and Kachanov (1983), Chudnovsky *et al.* (1987), Rose (1986) and Rubinstein (1986). Recently, Gong and Horii (1989) have derived a general solution to the interaction model for combined mode I and II loadings and discussed the accuracy of some of the previous solutions. With the aid of the leading order explicit solution, Gong and Horii (1989) were able to identify the specific regions of shielding and amplification associated with mode I loading. Their work was subsequently extended by Meguid *et al.* (1990) to provide all possible regions as well as contour levels of shielding and amplification with independent and coupled mode I and mode II loadings.

A limited number of articles has dealt with the corresponding mode III problem for very simplified configurations, for which it was possible to obtain closed-form exact solutions. Smith (1983) derived an exact solution for the stress intensity factor of the main crack in the presence of a collinear circular hole, while Turska-Klebek and Sokolowski (1984) obtained the solutions for collinear and vertical microcracks ahead of the main crack. More recently, Chiang (1986) has considered a slightly more general case of a collinear elliptical hole.

The purpose of the present study is to provide a general solution to the antiplane problem of the interaction between a semi-infinite main crack and an arbitrarily located and oriented elliptical hole. The analysis is based on the superposition principle and the appropriate complex potentials for the antiplane problem. The solution to the problem is obtained by superimposing three subproblems, each of which contains either the main crack or the elliptical hole. In the present formulation, the stress-free condition of the main crack is automatically satisfied, while the free elliptical hole condition due to Isida (1973) enabled the development of the relevant consistency equations leading to the determination of the unknown coefficients in the corresponding complex potentials.

The general plan of the article is as follows. Section 2 provides some of the basic equations which are fundamental to the current formulation, while the detailed derivations of the current antiplane problem are given in Section 3. In Section 4, the present solutions are verified by comparison with existing exact solutions. Numerical examples are provided to show the effect of geometry, location and orientation of microdefect upon the stress intensity factor at the main crack, K_{III}^{M}. Shielding and amplification effects resulting from the presence of the microdefect are also examined.

2. BASIC EQUATIONS IN ANTIPLANE ELASTICITY

The situation envisaged initially is that of a main crack existing within an infinite solid deforming under mode III loading conditions, as depicted in Fig. 1. In considering the antiplane elasticity problem, the non-vanishing stress and displacement components can be expressed in terms of one complex potential, Φ:

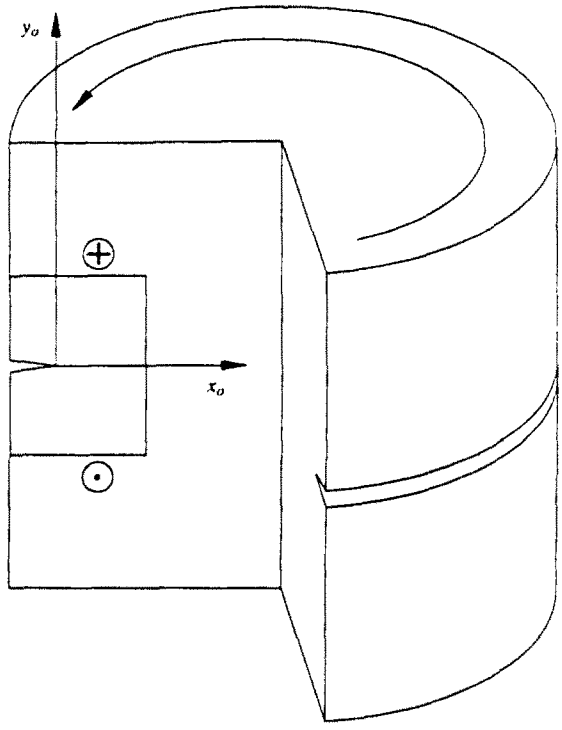

Fig. 1. Schematic representation of a crack under mode III loading.

$$\tau_{xz} - i\tau_{yz} = \Phi'(z),$$

$$w = \frac{1}{2G}[\Phi(z) + \overline{\Phi(z)}],$$

$$z = x + iy \quad \text{and} \quad i = \sqrt{-1}, \tag{1}$$

where τ_{xz} and τ_{yz} are the shear stresses, w is the displacement along the z-axis and G is the shear modulus. The overbar represents the complex conjugate and prime denotes the derivative with respect to the argument. The subscript z denotes the z-axis which should be distinguished from the complex variable $z = x + iy$. If the xy coordinate system is now rotated about the z-axis through an angle ϕ to form new coordinate axes m and n, then the corresponding transformation equation for the respective stresses τ_{mz} and τ_{nz} is:

$$\tau_{mz} - \tau_{nz} = e^{i\phi}(\tau_{xz} - \tau_{yz}) = e^{i\phi}\Phi'(z). \tag{2}$$

Now, consider the case of a single crack in an infinite solid lying on the interval $(-a, a)$ of the x-axis with the prescribed stress $\tau_{yz} = q(x)$ acting on the crack surfaces. The complex potential corresponding to the above loading is

$$\Phi'(z) = -\frac{1}{\pi\sqrt{z^2 - a^2}} \int_a^a \frac{\sqrt{x^2 - a^2}\, q(x)}{x - z}\, dx, \tag{3}$$

which simplifies to

$$\Phi'(z) = -\frac{1}{\pi\sqrt{z}} \int_0^\infty \frac{\sqrt{x}\, q(x)}{x - z}\, dx, \tag{4}$$

for a semi-infinite crack lying on the interval $(-\infty, 0)$.

Next, consider the case of a free elliptical hole having its centre at the origin and the major and minor diameters $(2a, 2b)$ along the x- and y-axes, respectively. Using the technique of conformal transformation and the method of Laurent series expansion (Isida, 1973), the general form of the complex potential for the free elliptical hole can be written as

$$\Phi(z) = \sum_{n=0}^{t} [(F_n^{\cdot} + iF_n^{*})(z/d)^{-(n+1)} + (M_n^{\cdot} + iM_n^{*})(z/d)^{n+1}], \tag{5}$$

where dots and asterisks denote real and imaginary parts, respectively, and d is some reference length. The coefficients of negative powers of eqn (5) can be expressed in terms of those of positive powers as

$$F_{2n}^{\cdot} = -\sum_{p=0}^{t} \lambda^{2n+2p+2} P_{2p}^{2n} M_{2p}^{\cdot}$$

$$F_{2n+1}^{\cdot} = -\sum_{p=0}^{t} \lambda^{2n+2p+4} P_{2p+1}^{2n+1} M_{2p+1}^{\cdot}$$

$$F_{2n}^{*} = -\sum_{p=0}^{t} \lambda^{2n+2p+2} Q_{2p}^{2n} M_{2p}^{*}$$

$$F_{2n+1}^{*} = -\sum_{p=0}^{t} \lambda^{2n+2p+4} Q_{2p+1}^{2n+1} M_{2p+1}^{*} \tag{6}$$

where

$$\begin{Bmatrix} P_{2p}^{2n} \\ Q_{2p}^{2n} \end{Bmatrix} = \frac{(1+\varepsilon)^{n+p+1}}{2^{2p+1}} \sum_{m=0}^{n-p} \binom{2p+1}{p-m} [(1-\varepsilon)^{n+p+1} \mp (1+\varepsilon)^{2m+1}(1-\varepsilon)^{n+p-2m}] A_{n,m,2m+1}$$

$$\begin{Bmatrix} P_{2p+1}^{2n+1} \\ Q_{2p+1}^{2n+1} \end{Bmatrix} = \frac{(1+\varepsilon)^{n+p+2}}{2^{2p+2}} \sum_{m=0}^{n-p} \binom{2p+2}{p-m} [(1-\varepsilon)^{n+p+2} \mp (1+\varepsilon)^{2m+2}(1-\varepsilon)^{n+p-2m}] A_{n,m,2m+2} \tag{7}$$

with

$$A_{n,m,2m+1} = \frac{2m+1}{2^{2n+1}(2n+1)} \binom{2n+1}{n-m}$$

$$A_{n,m,2m+2} = \frac{2m+2}{2^{2n+2}(2n+2)} \binom{2n+2}{n-m}$$

$$\lambda = a/d \quad \text{and} \quad \varepsilon = b/a. \tag{8}$$

In eqn (7), a smaller value of the summation upper limit (n or p) is implied.

3. MATHEMATICAL FORMULATION

Consider now the present problem of an infinitely extended solid containing a semi-infinite main crack and an arbitrarily located and oriented elliptical hole near its tip, as shown in Fig. 2. The undisturbed stress field in the absence of the elliptical hole is given by the singular elastic field corresponding to the applied stress intensity factor, K_{III}. The origins of two rectangular coordinate systems x_0y_0 and xy are taken at the tip of the main crack and the centre of the elliptical hole with its major and minor diameters ($2a$, $2b$) oriented along the x- and y-axes. The distance between the tip of the main crack and the centre of the elliptical hole is denoted by d, the angle measured from x_0-axis to the line connecting the tip of the main crack and the centre of the elliptical hole by θ, and the orientation angle of the elliptical hole by ϕ.

Now, the total complex potential Φ for the problem is considered as being the sum of three functions; namely

$$\Phi = \Phi_1 + \Phi_2 + \Phi_3, \tag{9}$$

which correspond to three separate subproblems, as illustrated in Fig. 3.

In subproblem 1, the main crack is subjected to the applied stress intensity factor K_{III}. The stress field near the tip of the main crack is given by the singular near-tip stress field. The corresponding stress function Φ_1 for subproblem 1 is given by

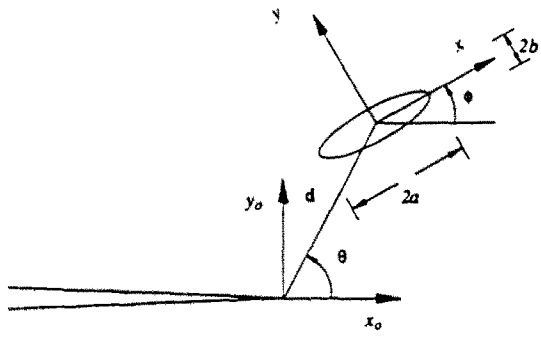

Fig. 2. Arbitrarily located and oriented elliptical hole near the tip of a main crack.

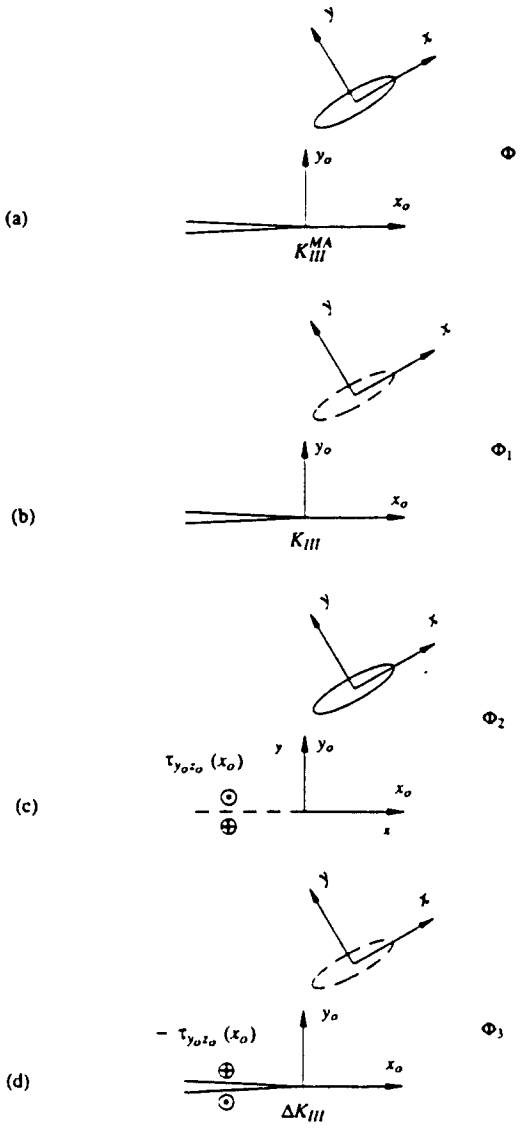

Fig. 3. The superposition principle utilizing three subproblems. (a) The original problem. (b) Subproblem 1. (c) Subproblem 2. (d) Subproblem 3.

$$\Phi_1'(z_0) = -\frac{iK_{III}}{\sqrt{2\pi z_0}}$$

$$z_0 = x_0 + iy_0 \quad \text{and} \quad i = \sqrt{-1}, \tag{10}$$

where prime denotes derivative with respect to the corresponding argument, z_0.

Subproblem 2 considers the case of an infinite solid containing a single elliptical hole described by the following stress function Φ_2 which has singularities within the hole (Isida, 1973),

$$\Phi_2(z) = \sum_{n=0}^{\infty} F_n (z/d)^{-(n+1)} \tag{11}$$

with $z = x + iy$ and the unknown coefficients ($F_n = F_n' + iF_n''$) to be determined. From (2) and (11), the stress along the position of the main crack is obtained as

$$\tau_{r_0 z_0}(x_0) = \frac{i}{2}[e^{-i\phi}\Phi_2'(z) - e^{i\phi}\Phi_2'(z)], \tag{12}$$

with $z = (x_0 - \xi)e^{i\phi}$ and $\xi = de^{i\theta}$.

In subproblem 3, the main crack is loaded by the traction $-\tau_{r_0 z_0}(x_0)$. From (4), the stress function for subproblem 3 is given by

$$\Phi_3'(z_0) = \frac{1}{\pi\sqrt{z_0}}\int_0^a \frac{\sqrt{x_0}\,\tau_{r_0 z_0}(x_0)}{x_0 - z_0}\,dx_0. \tag{13}$$

The stress intensity factor for the main crack is obtained from

$$\Delta K_{III} = \sqrt{\frac{2}{\pi}}\int_0^a \frac{\tau_{r_0 z_0}(-x_0)}{\sqrt{x_0}}\,dx_0. \tag{14}$$

Substituting (12) into (13), $\Phi_3'(z_0)$ can be obtained as

$$\Phi_3'(z_0) = \frac{1}{2\sqrt{z_0}}\sum_{n=0}^{r}(n+1)d^{n+1}\{F_n e^{i[(n+1)\theta]}S_{n+1}(z_0,\xi) - \bar{F}_n e^{-i[(n+1)\theta]}S_{n+1}(z_0,\bar{\xi})\}, \tag{15}$$

where

$$S_0(z_0,\xi) = \frac{1}{\sqrt{\xi}+\sqrt{z_0}},$$
$$S_n(z_0,\xi) = S_0(z_0,\xi)\sum_{t=1}^{n} S_{n-t}(z_0,\xi)Q_t(\xi), \tag{16}$$

with

$$Q_t(\xi) = \frac{(-1)^t}{2t}p_{t-1}\frac{\sqrt{\xi}}{\xi^t} \tag{17}$$

and

$$p_t = \frac{(2t)!}{2^{2t}(t!)^2}. \tag{18}$$

Equations (11), (12) and (14) yield the following expression for the stress intensity factor at the tip of the main crack:

$$\Delta K_{III} = \sum_{n=0}^{r}(-1)^n(n+1)p_{n+1}\sqrt{\frac{2\pi}{d}} \times \{F_n^* \sin[(n+1)\phi - (n+\tfrac{1}{2})\theta] + F_n^* \cos[(n+1)\phi - (n+\tfrac{1}{2})\theta]\}. \tag{19}$$

It is now appropriate to consider the superposition of the three subproblems. The total complex potential Φ satisfies the traction-free condition along the main crack. However, the traction-free condition for the elliptical hole should be examined. Since the free-hole condition (5) is given in terms of the local coordinates, it is necessary to express the total complex potential Φ as a function of z. The transformation relation between main crack and microdefect coordinates is given by

$$z_0 = z\,e^{i\phi} + \xi. \tag{20}$$

Substituting (20) into (10) and (15), and combining with (11), the total complex potential Φ is reduced to the same form as eqn (5), as follows:

$$\Phi(z) = \sum_{n=0}^{r} [(F_n^* + iF_n^*)(z/d)^{-(n+1)} + (M_n^* + iM_n^*)(z/d)^{n+1}], \tag{21}$$

where

$$M_n^* = \frac{(-1)^{n+2} p_n K_{III}}{n+1} \sqrt{\frac{d}{2\pi}} \cdot \sin[(n+1)\phi - (n+\tfrac{1}{2})\theta] + \sum_{p=0}^{r} (a_{np} F_p^* + d_{np} F_p^*),$$

$$M_n^* = \frac{(-1)^{n+1} p_n K_{III}}{n+1} \sqrt{\frac{d}{2\pi}} \cdot \cos[(n+1)\phi - (n+\tfrac{1}{2})\theta] + \sum_{p=0}^{r} (b_{np} F_p^* + c_{np} F_p^*). \tag{22}$$

The expressions for the coefficients a_{np}, b_{np}, c_{np} and d_{np} are provided in the Appendix.

Equations (22) and (6) constitute the necessary consistency equations for determining the unknown coefficients F_n^*, F_n^*, M_n^*, M_n^* $(n = 0, 1, 2, \ldots)$, which are solved with the aid of the following perturbation technique. Assume that all the unknown coefficients can be expressed as a power series in terms of (a/d) such that

$$F_{2n} = \sqrt{d} \sum_{q=n+1}^{r} F_{2n}^{*(2q)} (a/d)^{2q},$$

$$F_{2n+1} = \sqrt{d} \sum_{q=n+2}^{r} F_{2n+1}^{*(2q)} (a/d)^{2q},$$

$$M_n = \sqrt{d} \sum_{q=0}^{r} M_n^{(2q)} (a/d)^{2q}. \tag{23}$$

Substituting (23) into (6) and (22) and equating the coefficients of the same powers on both sides, the following recurrent formulae are obtained:

$$M_n^{*(0)} = \frac{(-1)^{n+2} p_n K_{III}}{n+1} \sqrt{\frac{1}{2\pi}} \sin[(n+1)\phi - (n+\tfrac{1}{2})\theta],$$

$$M_n^{*(0)} = \frac{(-1)^{n+1} p_n K_{III}}{n+1} \sqrt{\frac{1}{2\pi}} \cos[(n+1)\phi - (n+\tfrac{1}{2})\theta],$$

$$F_{2n}^{*(2n+2)} = -P_0^{2n} M_0^{*(0)},$$

$$F_{2n}^{*(2n+2)} = -Q_0^{2n} M_0^{*(0)},$$

$$M_n^{*(2)} = a_{n0} F_0^{*(2)} + d_{n0} F_0^{*(2)},$$

$$M_n^{*(2)} = b_{n0} F_0^{*(2)} + c_{n0} F_0^{*(2)},$$

$$F_{2n}^{*(2n+2q)} = -\sum_{p=0}^{q-1} P_{2p}^{2n} M_{2p}^{*(2q-2p-2)},$$

$$F_{2n}^{*(2n+2q)} = -\sum_{p=0}^{q-1} Q_{2p}^{2n} M_{2p}^{*(2q-2p-2)},$$

$$F_{2n+1}^{*(2n+2q)} = -\sum_{p=0}^{q-2} P_{2p+1}^{2n+1} M_{2p+1}^{*(2q-2p-4)},$$

$$F_{2n+1}^{*(2n+2q)} = -\sum_{p=0}^{q-2} Q_{2p+1}^{2n+1} M_{2p+1}^{*(2q-2p-4)},$$

$$M_n^{*(2q)} = \sum_{p=0}^{2q-2} [a_{np} F_p^{*(2q)} + d_{np} F_p^{*(2q)}],$$

$$M_n^{*(2q)} = \sum_{p=0}^{2q-2} [b_{np} F_p^{*(2q)} + c_{np} F_p^{*(2q)}]$$

$$(q = 2, 3, 4, \ldots). \tag{24}$$

Using the above relations, the expansion coefficients in eqns (23) can be calculated to as many terms as required.

The stress intensity factor for the main crack is thus given by

$$K_{\mathrm{III}}^{M\,t} = K_{\mathrm{III}} + \Delta K_{\mathrm{III}}, \tag{25}$$

where ΔK_{III} is obtained from (19) with F_n^* and F_n^{**} determined from (23) and (24). It is observed from (19) and (23) that ΔK_{III} can be expressed in terms of even powers $(a/d)^{2N}$ $(N = 1, 2, 3, \ldots)$. Taking the dominant terms, $N = 1$ and $N = 2$ in (25), the following normalized closed-form expressions for the first and second order approximate solutions are obtained; namely

$$K_{\mathrm{III}}^{M\,t}/K_{\mathrm{III}} = 1 + \left(\frac{a}{d}\right)^2 G(\theta, \phi, \varepsilon) \quad (N = 1) \tag{26}$$

$$K_{\mathrm{III}}^{M\,t}/K_{\mathrm{III}} = 1 + \left(\frac{a}{d}\right)^2 G(\theta, \phi, \varepsilon) + \left(\frac{a}{d}\right)^4 H(\theta, \phi, \varepsilon) \quad (N = 2) \tag{27}$$

where $G(\theta, \phi, \varepsilon)$ and $H(\theta, \phi, \varepsilon)$ are derived explicitly as

$$G(\theta, \phi, \varepsilon) = \tfrac{1}{8}[\cos(2\phi - 2\theta)(1 - \varepsilon^2) + \cos\theta\,(1 + \varepsilon)^2]$$

and

$$\begin{aligned} H(\theta, \phi, \varepsilon) = \frac{(1+\varepsilon)^2}{128}\Bigg[& \frac{(1-\varepsilon)\cos(2\phi - 2\theta) + (1+\varepsilon)\cos\theta}{1+\cos\theta} + 6 + \varepsilon\cos(\theta\ 2) \\ & + (1-\varepsilon)\cos\theta\cos(2\phi - \tfrac{5}{2}\theta) + 3(1-\varepsilon)\cos(2\phi - \theta) + 15(1-\varepsilon)\cos(2\phi - 3\theta) \\ & - 15(1-\varepsilon^2)\sin(3\phi - \tfrac{7}{2}\theta)\sin\left(\phi - \frac{\theta}{2}\right) - 3(1-\varepsilon^2)\cos^2(2\phi - \tfrac{3}{2}\theta) \\ & - 3(1-\varepsilon^2)\sin(\phi - \tfrac{3}{2}\theta)\sin(3\phi - \tfrac{5}{2}\theta) - (1-\varepsilon^2)\sin(\phi - \tfrac{3}{2}\theta) \\ & \times \sin\left(\phi - \frac{\theta}{2}\right)\cos(2\phi - \tfrac{5}{2}\theta)\Bigg]. \end{aligned} \tag{28}$$

4. RESULTS AND DISCUSSION

This section is divided into two main parts. The first presents results with a view to verifying the preceding analysis, while the second examines the effect of the pertinent parameters upon the stress intensity factor at the main crack.

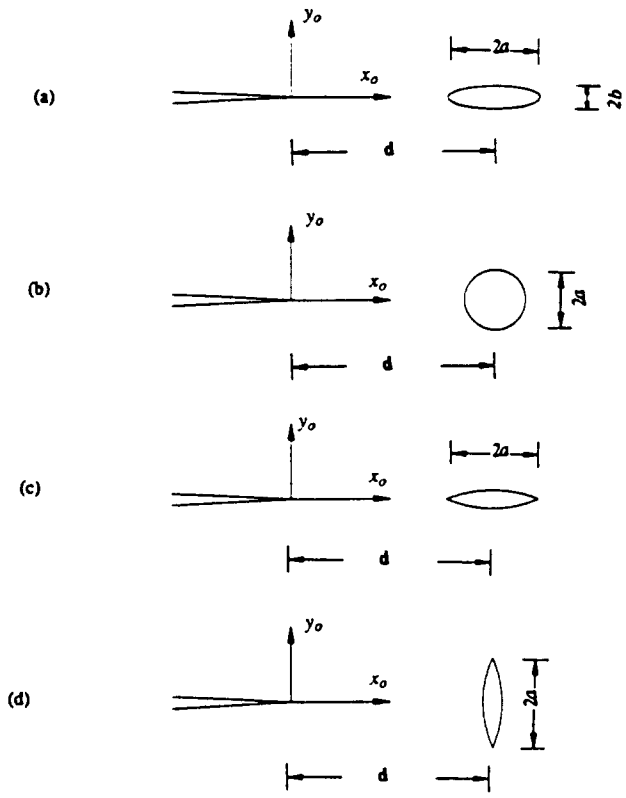

Fig. 4. Special configurations of elliptical holes ahead of a main crack for which exact solutions exist. (a) Collinear elliptical hole. (b) Collinear circular hole. (c) Collinear microcrack. (d) Vertical microcrack.

To enable comparisons with existing exact solutions, the configurations shown in Fig. 4 were considered. In the case of a collinear elliptical hole ahead of the main crack (Fig. 4a), the closed-form solution derived by Chiang (1986)† can be written in a compact form, using the present notation, as follows:

$$\frac{K_{III}^{MA}}{K_{III}} = \sqrt{\frac{G(1+h)}{h-1}}\,\frac{E(\kappa)}{K(\kappa)}, \tag{29}$$

with

$$\kappa = \sqrt{\frac{2}{1+h}},$$

$$h = \frac{1}{4\lambda}[(1+N)+4\lambda^2(1+N)^{-1}],$$

$$G = \frac{1}{2N}[(1+N)-4\lambda^2(1+N)^{-1}], \tag{30}$$

and

$$N = \sqrt{1+(\varepsilon^2-1)(a/d)^2}, \quad \lambda = \left(\frac{1+\varepsilon}{2}\right)(a/d), \quad \varepsilon = b/a,$$

where K and E denote the complete elliptical integrals of the first and second kind, respectively.

† There are two misprints in eqns (7) and (13) in Chiang (1986).

Expanding (29) into Taylor series with respect to (a/d), we obtain

$$K_{III}^{M}/K_{III} = 1 + \tfrac{1}{4}(1+\varepsilon)\left(\frac{a}{d}\right)^2 + \frac{(1+\varepsilon)^2}{128}(23-18\varepsilon+3\varepsilon^2)\left(\frac{a}{d}\right)^4 + \cdots. \tag{31}$$

Substituting $\theta = 0$ and $\phi = 0$ into (27), it is confirmed that the present solution coincides with (31). Additionally, the respective configurations of a collinear circular hole ($\varepsilon = 1$) and a collinear microcrack ($\varepsilon = 0$), depicted in Fig. 4b and c, were also confirmed in a similar manner.

Figure 4d shows a vertical microcrack ahead of the main crack. The closed-form exact solution for this problem was given by Turska-Klebek and Sokolowski (1984) as

$$\frac{K_{III}^{M}}{K_{III}} = \frac{\lambda + \sqrt{1+\lambda^2}\,E(\kappa)}{(1+\lambda^2)^{1/4}\,K(\kappa)}, \tag{32}$$

where

$$\kappa = \sqrt{\frac{2\lambda}{\lambda+\sqrt{1+\lambda^2}}} \quad \text{and} \quad \lambda = \frac{a}{d}.$$

Expanding (32) into Taylor series with respect to $\lambda = a/d$ leads to

$$K_{III}^{M}/K_{III} = 1 + \frac{3}{128}\left(\frac{a}{d}\right)^4 + \cdots. \tag{33}$$

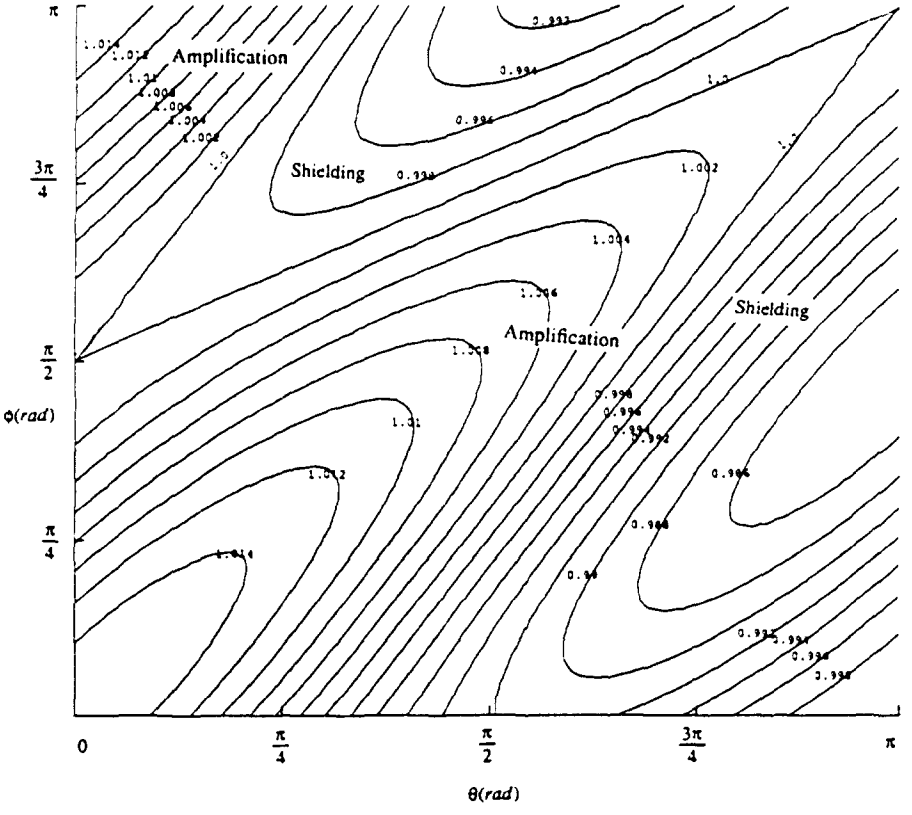

Fig. 5. Contour representation of normalized stress intensity factor K_{III}^{M}/K_{III} as a function of location and orientation of a microcrack; $\varepsilon = 0$.

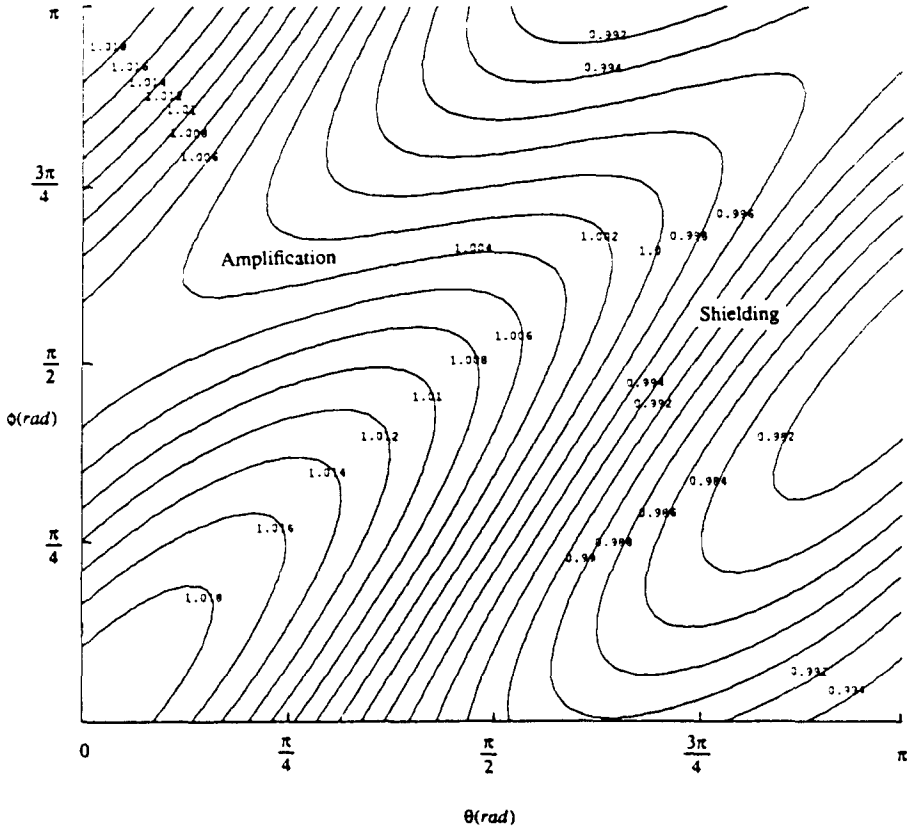

Fig. 6. Contour representation of normalized stress intensity factor $K_{III}^{M,I}/K_{III}$ as a function of location and orientation of an elliptical hole; $\varepsilon = 1/4$.

Substituting $\theta = 0$, $\phi = \pi/2$ and $\varepsilon = 0$ into (27), it is again confirmed that the present solution coincides with (33). It is worth noting that the above equation can also be directly derived from eqn (31), with the appropriate substitutions.

Typical results of the stress intensity factor predicted by the present first and second order solutions are compared with the exact solutions of eqn (29) for a collinear elliptical hole in Table 1. The table shows that the presence of a collinear cut out, whether an elliptical hole, a circular hole or a microcrack, introduces an increase in the stress intensity factor of the main crack. Furthermore, it can be seen that the circular cut out ($\varepsilon = 1$) provides the largest increase in the normalized stress intensity factor ($K_{III}^{M,I}/K_{III}$), for a given (a/d).

Table 1. Normalized stress intensity factor ($K_{III}^{M,I}/K_{III}$) as a function of location (a/d) and aspect ratio ($\varepsilon = b/a$) of a collinear elliptical hole

	Exact [eqn (29)]			First order [eqn (26)]			Second order [eqn (27)]		
a/d	$\varepsilon = 0$	$\varepsilon = 1/2$	$\varepsilon = 1$	$\varepsilon = 0$	$\varepsilon = 1/2$	$\varepsilon = 1$	$\varepsilon = 0$	$\varepsilon = 1/2$	$\varepsilon = 1$
0	1.000	1.000	1.000	1.000	1.000	1.000	1.000	1.000	1.000
0.1	1.003	1.004	1.005	1.003	1.004	1.005	1.003	1.004	1.005
0.2	1.010	1.015	1.020	1.010	1.015	1.020	1.010	1.015	1.020
0.3	1.024	1.036	1.047	1.022	1.034	1.045	1.024	1.036	1.046
0.4	1.046	1.068	1.087	1.040	1.060	1.080	1.045	1.067	1.086
0.5	1.077	1.114	1.144	1.063	1.094	1.125	1.074	1.110	1.141
0.6	1.123	1.182	1.225	1.090	1.135	1.180	1.113	1.169	1.212
0.7	1.195	1.292	1.343	1.123	1.184	1.245	1.166	1.246	1.305
0.8	1.319	1.447	1.532	1.160	1.240	1.320	1.234	1.346	1.422
0.9	1.591	1.881	1.921	1.203	1.304	1.422	1.320	1.474	1.569

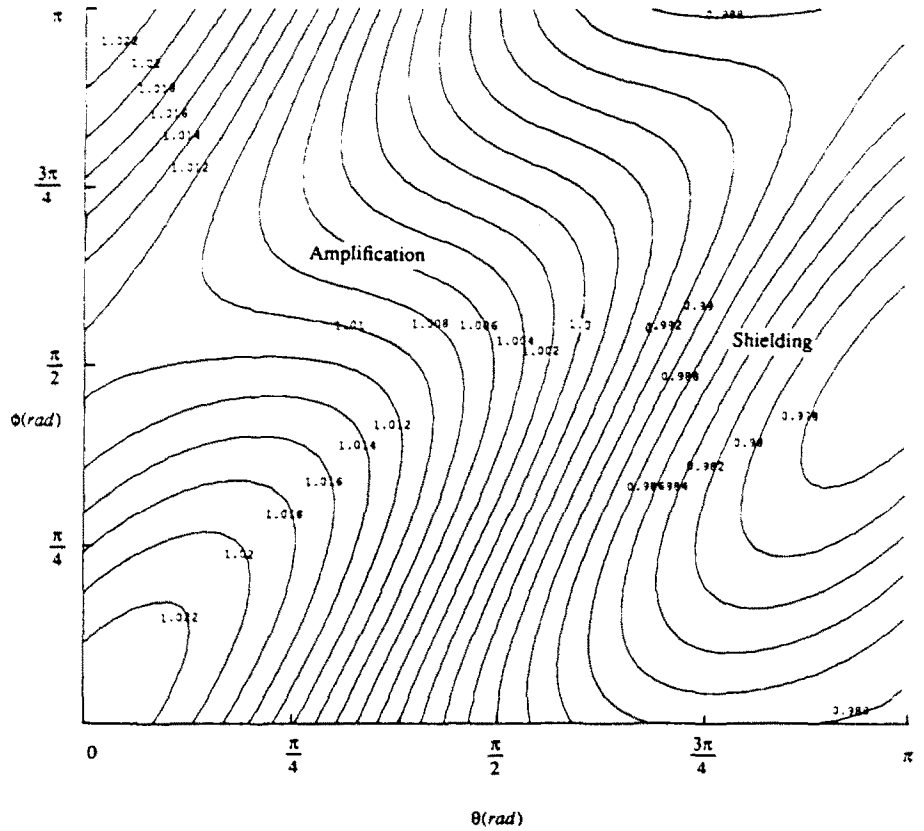

Fig. 7. Contour representation of normalized stress intensity factor $K_{III}^{M,I}/K_{III}$ as a function of location and orientation of an elliptical hole; $\varepsilon = 1/2$.

Two further observations can be made from the table. The first is that provided a/d is relatively small, the first and second order solutions generally underestimate the exact solution by a very small amount. The second is that the accuracy of the proposed approximate solutions depends upon the relative position of the microdefect, a/d. For example, in the case of $a/d = 0.9$, where the microdefect is very close to the crack-tip, the maximum error resulting from the use of the second order solution is 21%. Nevertheless, if $a/d \leqslant 0.5$, then the maximum error resulting from the use of the first order solution is within 2% of exact solutions.

Consider now the case of an arbitrarily located and oriented elliptical hole near the tip of a main crack. The present formulation predicts the dependence of the normalized stress intensity factor ($K_{III}^{M,I}/K_{III}$) upon the location ($a/d, \theta$), orientation (ϕ) and aspect ratio ($\varepsilon = b/a$) of the elliptical hole. For a given elliptical hole (a/d, θ, ϕ and ε), it is now possible to compute the corresponding contour levels and the associated regions of shielding ($K_{III}^{M,I}/K_{III} < 1$) and amplification ($K_{III}^{M,I}/K_{III} > 1$). For simplicity, the first order solution [eqn (26)] was used in the analysis of a microdefect with $a/d = 1/4$. For this first order solution, the regions of shielding and amplification are independent of the ratio (a/d). Accordingly, setting $G(\theta, \phi, \varepsilon)$ of eqn (28) to zero is sufficient for determining the regions of shielding and amplification associated with mode III, as depicted in Figs 5–9 for different geometries of the microdefect.

Figure 5 shows the contour levels of $K_{III}^{M,I}/K_{III}$ and the associated regions of amplification and shielding under mode III loading for a microcrack ($\varepsilon = 0$). Depending upon the orientation ϕ and location of the microcrack θ, the stress intensity factor at the main crack may be increased or decreased as described by the four distinct regions of Fig. 5.

Figures 6–8 show the corresponding contour levels and regions of shielding and amplification for an arbitrarily oriented and located elliptical hole ($\varepsilon = 1/4$, $1/2$ and $3/4$),

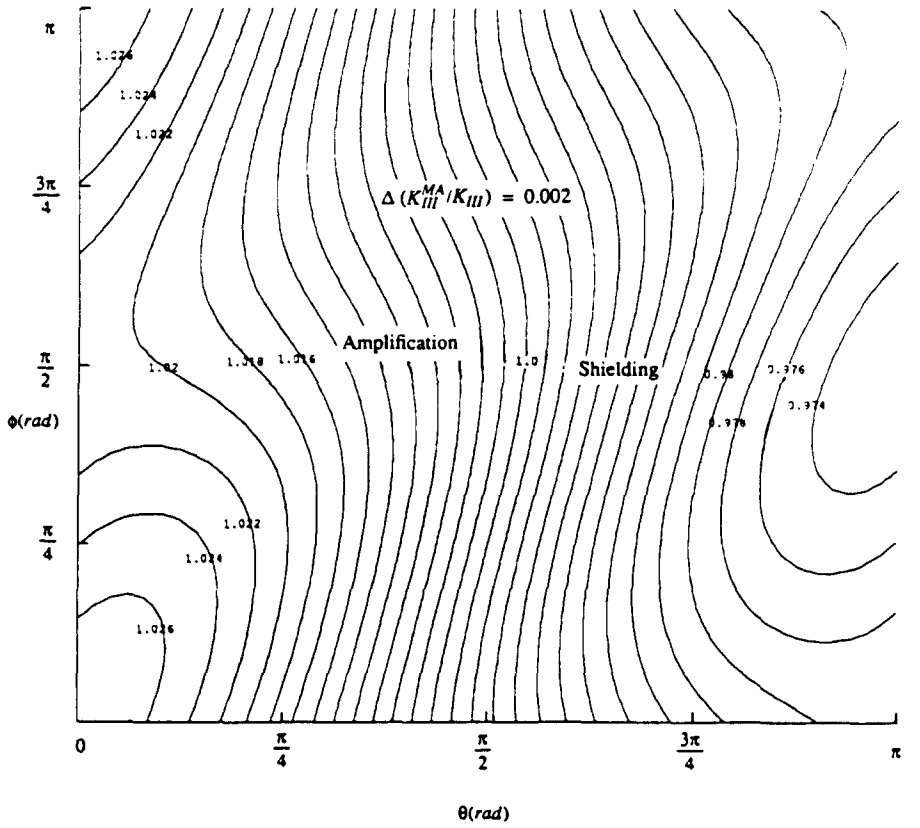

Fig. 8. Contour representation of normalized stress intensity factor K_{III}^{M}/K_{III} as a function of location and orientation of an elliptical hole; $\varepsilon = 3/4$.

while Fig. 9 shows the corresponding results for a circular hole ($\varepsilon = 1$). In these cases, only two regions of shielding and amplification are now identified. These figures also indicate that amplification changes to shielding as θ varies from 0 to π. Furthermore, the trajectories of the normalized stress intensity factor at the main crack are drastically influenced by the geometry of the hole. In the case of the circular hole, the trajectories become independent of the "defect orientation", ϕ, as would be expected due to the symmetric nature of the hole. This trend can also be observed for elliptical holes with relatively large aspect ratios, as depicted in Fig. 8 for $\varepsilon = 3/4$.

5. CONCLUSIONS

In this article, a general solution to the interaction between a main crack and an arbitrarily located and oriented elliptical hole under mode III loading was developed. The analysis was based on the complex variable formulation and supported by the superposition principle. In particular, the stress intensity factor of the main crack was obtained in general asymptotic forms, and explicit analytical first and second order solutions were also provided. The present solutions agree with Taylor expansions of exact solutions for the special cases corresponding to a collinear elliptical hole with different aspect ratios.

The results of the work also reveal that depending upon the aspect ratio, location and orientation of the elliptical hole, shielding and amplification effects may become prevalent. In the case of shielding, this provides a remarkable toughening effect, while in the case of amplification it provides an undesirable weakening effect. The work provides a useful quantitative design tool and a valuable insight into main crack–microdefect interaction phenomena in brittle materials.

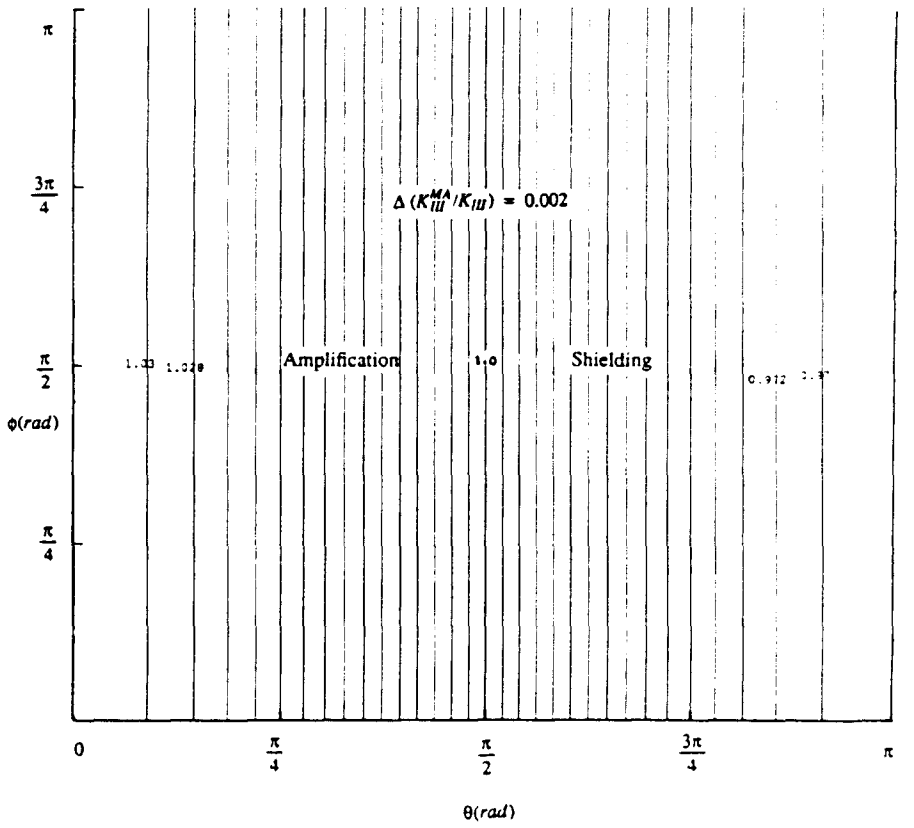

Fig. 9. Contour representation of normalized stress intensity factor K_{III}^{M}/K_{III} as a function of location and orientation of a circular hole; $\varepsilon = 1$.

Acknowledgements—The financial support provided by the Natural Sciences and Engineering Research Council and Energy, Mines and Resources of Canada is gratefully acknowledged. The authors are also grateful for the financial support provided by Dean G. W. Heinke, Faculty of Applied Science and Engineering, University of Toronto, through the Edgar McAllister Fund.

REFERENCES

Charalambides, P. and McMeeking, R. M. (1988). Near tip mechanics of stress induced microcracking in brittle materials. *J. Am. Ceram. Soc.* **71**, 465–472.

Chiang, C. R. (1986). The effect of an elliptical hole on the stress intensity factor of a macrocrack. *Engng Fracture Mech.* **25**, 17–21.

Chudnovsky, A. and Kachanov, M. (1983). Interaction of a crack with a field of microcracks. *Int. J. Engng Sci.* **21**, 1009–1018.

Chudnovsky, A., Dolgopolsky, A. and Kachanov, M. (1987). Elastic interaction of a crack with a microcrack array. *Int. J. Solids Structures* **23**, 1–21.

Claussen, N., Steeb, J. and Pabst, R. F. (1977). Effect of induced microcracking on the fracture toughness of ceramics. *Bull. Am. Ceram. Soc.* **56**, 559–562.

Evans, A. G. and Faber, K. T. (1984). Crack-growth resistance of microcracking brittle materials. *J. Am. Ceram. Soc.* **67**, 255–260.

Evans, A. G. and Fu, Y. (1985). Some effects of microcracks on the mechanical properties of brittle solids—II. Microcrack toughening. *Acta Metall.* **33**, 1515–1523.

Gong, S. X. and Horii, H. (1989). General solution to the problem of microcracks near the tip of a main crack. *J. Mech. Phys. Solids* **37**, 27–46.

Hoagland, R. G. and Embury, J. D. (1980). A treatment of inelastic deformation around a crack tip due to microcracking. *J. Am. Ceram. Soc.* **63**, 404–410.

Hoagland, R. G., Hahn, G. T. and Rosenfield, A. R. (1973). Influence of microstructure on fracture propagation in rock. *Rock Mech.* **5**, 77–106.

Hutchinson, J. W. (1987). Crack tip shielding by micro-cracking in brittle solids. *Acta Metall.* **35**, 1605–1619.

Isida, M. (1973). Method of Laurent series expansion for internal crack problems. In *Methods of Analysis and Solutions of Crack Problems* (Edited by G. C. Sih), pp. 56–130. Noordhoff, Leyden.

Meguid, S. A., Gong, S. X. and Gaultier, P. E. (1990). Main crack microcrack interaction: shielding and amplification. *University of Toronto, UTME Publications* **102**, 1990.

Ortiz, M. (1987). Continuum theory of crack shielding in ceramics. *J. Appl. Mech.* **54**, 54–58.

Ortiz, M. (1988). Microcrack coalescence and macroscopic crack growth initiation in brittle solids. *Int. J. Solids Structures*. **24**, 231–250.
Rose, L. R. F. (1986). Microcrack interaction with a main crack. *Int. J. Fracture* **31**, 233–246.
Rubinstein, A. A. (1986). Macrocrack–microdefect interaction. *J. Appl. Mech.* **53**, 505–510.
Rühle, M., Evans, A. G., McMeeking, R. M., Charalambides, P. G. and Hutchinson, J. W. (1987). Microcrack toughening in alumina zirconia. *Acta Metall.* **35**, 1701–1710.
Smith, E. (1983). The effect of a circular cylindrical hole on the stress intensity at a crack tip. *Arch. Mech.* **35**, 741–746.
Turska-Klebek, E. and Sokolowski, M. (1984). On the influence of defects upon stress concentration at the crack. *Arch. Mech.* **36**, 121–126.

APPENDIX

Substituting (20) into (15), the stress potential Φ_1 can be written in terms of z as follows:

$$\Phi_1(z) = \sum_{n=0}^{\infty} \sum_{p=0}^{n} [F_p R_{np} + \bar{F}_p T_{np}](z-d)^{n+1}, \tag{A1}$$

where R_{np} and T_{np} are two complex functions defined by

$$R_{np} = \frac{(-1)^n(p+1)}{2(n+1)} e^{i[(p+n+2)\alpha+\beta]} \sum_{t=0}^{n} \frac{(-1)^t p_{n-t}}{\zeta^{2(n-t)} \omega^t} S_{p+1,t}(\xi, \bar{\xi}) \tag{A2}$$

and

$$T_{np} = \frac{(-1)^{n+1}(p+1)}{2(n+1)} e^{i[(p-n)\alpha+\beta]} \sum_{t=0}^{n} \frac{(-1)^t p_{n-t}}{\zeta^{2(n-t)} \omega^t} S_{p+1,t}(\xi, \bar{\xi}), \tag{A3}$$

with

$$\begin{aligned}
S_{00}(\xi, \bar{\xi}) &= \frac{1}{\omega \bar{\xi} + \omega^3 \xi} \\
S_{0t}(\xi, \bar{\xi}) &= S_{00}(\xi, \bar{\xi}) \sum_{i=0}^{t-1} S_{0i}(\xi, \bar{\xi}) Q_{t-i}(\bar{\xi}) \\
S_{0p}(\xi, \bar{\xi}) &= S_{00}(\xi, \bar{\xi}) \sum_{i=0}^{p-1} S_{0i}(\xi, \bar{\xi}) Q_{p-i}(\bar{\xi}) \\
S_{tp}(\xi, \bar{\xi}) &= S_{00}(\xi, \bar{\xi}) \left[\sum_{i=0}^{t-1} S_{ip}(\xi, \bar{\xi}) Q_{t-i}(\bar{\xi}) + \sum_{i=0}^{p-1} S_{ti}(\xi, \bar{\xi}) Q_{p-i}(\bar{\xi}) \right]
\end{aligned} \tag{A4}$$

where $Q_i(\xi)$ is given by (17), and $\xi = e^{i\alpha}$.

Then the coefficients a_{np}, b_{np}, c_{np} and d_{np} in eqn (22) are evaluated as

$$\begin{aligned}
a_{np} &= \mathrm{Re}\,(R_{np} + T_{np}) \\
b_{np} &= \mathrm{Im}\,(R_{np} + T_{np}) \\
c_{np} &= \mathrm{Re}\,(R_{np} - T_{np}) \\
d_{np} &= -\mathrm{Im}\,(R_{np} - T_{np}),
\end{aligned} \tag{A5}$$

where Re and Im denote the real and imaginary parts of a complex variable, respectively.